IEEE Access
Multidisciplinary : Rapid Review : Open Access Journal

Received December 25, 2019, accepted January 15, 2020, date of publication January 21, 2020, date of current version February 4, 2020.

Digital Object Identifier 10.1109/ACCESS.2020.2968379

Modulated Model-Free Predictive Control With Minimum Switching Losses for PMSM Drive System

YUCHEN WANG, HONGMEI LI, RUNDONG LIU, LIGUO YANG, AND XIANLING WANG
Department of Electrical Engineering and Automation, Hefei University of Technology, Hefei 230009, China

Corresponding author: Hongmei Li (hongmei.li@hfut.edu.cn)

This work was supported in part by the National Natural Science Foundation of China under Grant 51877064, and in part by the Anhui Provincial Key Research and Development Program Funding under Grant 1804a09020092.

ABSTRACT A modulated model-free predictive control with minimum switching losses (MSL-MMFPC) is proposed to improve the steady-state performance and reduce the switching losses for a permanent magnet synchronous motor (PMSM) drive system. Firstly, two adjacent current vectors are determined based on the predefined first-level cost function, and then, make the current vector at the next control period equal to the reference current vector by modulating the selected current vectors properly. Additionally, in order to keep optimal control performance also in the over-modulation region, a new rotating coordinate frame is used to adjust the optimal voltage vector. Then, the second-level cost function is designed to select the optimal voltage vector sequence, so that the switching of a VSI leg does not happen during the phase-current maximum, which can reduce the switching losses of the inverter. The simulation and experimental results verify the effectiveness of the proposed control method.

INDEX TERMS PMSM drive system, modulated model-free predictive control, optimal voltage vector, over-modulation operation, minimum switching losses.

I. INTRODUCTION

In recent years, permanent magnet synchronous motors (PMSMs) have been widely used in electric vehicles and other industry fields due to its high power/torque density and high efficiency. With the rapid development of microprocessors, model predictive control (MPC) becomes a typical optimal control algorithm and receives more and more attention in PMSM drive systems [1]. MPC can be divided into two types: continuous control set model predictive control (CCS-MPC) and finite control set model predictive control (FCS-MPC) [2]. FCS-MPC effectively utilizes the discrete nature of the inverters and predicts the future behavior of the system variables, and then the optimal switching state will be chosen through the predefined cost function and applied in the next control period. Therefore, it is easier to realize nonlinear multi-objective and multi-constrained control [3]. However, since the FCS-MPC depends on the accuracy of the mathematical model, there are various uncertainties and disturbances in PMSM drive systems, which lead to a degradation of control performance.

The associate editor coordinating the review of this manuscript and approving it for publication was Jinquan Xu.

The model-free control (MFC) [4] establishes the ultra-local model online based on the input and output data of the controlled system, and it uses this ultra-local model to design the controller. This method gets rid of the dependence on the mathematical model of the system and has strong robustness. In [5], the model-free control is successfully applied to a deadbeat predictive current control of a surface mounted permanent magnet synchronous motor (SMPMSM) drive system, which effectively decreases the negative impact of inverter nonlinearity and motor parameter variation on the system performance.

In the conventional FCS-MPC, a modulator is lacked and only one basic voltage vector is applied for the entire control period, which will generate high current and torque ripple [6]. Therefore, the FCS-MPC often adopted a high sampling frequency to reduce current and torque ripples. Thus, how to improve the steady-state control performance of the conventional FCS-MPC without increasing the sampling frequency is a key technology to be solved urgently [7], [8].

In order to improve the steady-state control performance of the conventional FCS-MPC, there are several solutions proposed in recent years. In [9] and [10], a method to increase the FCS-MPC prediction horizon is used to improve the control performance. However, with the increase of prediction horizon, the control algorithm will become more complex, which will greatly increase the computation load of online optimization process. Another solution is to introduce a modulation strategy into FCS-MPC, such as duty cycle control [11], [12] and three-vector control [13]–[16]. Duty cycle control applies an active voltage vector and a zero voltage vector in one control period and it is an effective way to improve the steady-state performance of the conventional FCS-MPC. However, the duty cycle control cannot realize the current tracking without error theoretically. In order to realize no-error tracking control, the three-vector control method is proposed. In this method, two adjacent active voltage vectors and a zero voltage vector are applied in one control period. Although the three-vector control greatly improves the steady-state control performance of the controlled system, the calculation process is complicated. Deadbeat control [17] is a simple three-vector control and often used with space-vector pulse-width modulation (SVM). Although deadbeat control is an ideal control method for PMSM, it is dependent on the exact mathematical model of PMSM, and it is difficult to realize multi-objective and multi-constrained control.

In order to overcome the limitations above-mentioned, a method called modulated model predictive control (MMPC) is proposed recently [18]–[29], it integrates the SVM into FCS-MPC algorithms, and it retains the advantages of FCS-MPC as a multi-objective control but improve the performance of the controlled system. In [18]–[26], the duty cycles of basic voltage vectors are calculated by assuming that duty cycles are inversely proportional to their corresponding cost function values. However, it does not consider the directions of the predictive current error vectors; thus, the calculation of the duty cycles is inaccurate. In [27] and [28], the optimal voltage vector is obtained by the deadbeat predictive control, and then uses multiple cost function to select the optimal active voltage vectors and calculate their duty cycles. In [29], the torque tracking errors and MTPA control errors of all basic voltage vectors are predicted and can be recorded on an established two-dimensional coordinate system. Thus, the optimal voltage vector is the voltage vector corresponding to the origin of the two-dimensional coordinate and is calculated by the method of linear approximation and interpolation. Nevertheless, it does not present an optimized solution in the over-modulation region.

In the MMPC method above-mentioned, the duty cycle combination of all adjacent vectors needs to be calculated, which requires a large amount of calculation. Moreover, the switching frequency of the inverter is high in PMSM drive system, so reducing switching losses can effectively improve the system efficiency. Further research is required to analyze the use of MMPC in PMSM drive system.

The five-segment SVM strategy has the advantage of low switching frequency compared with seven-segment SVM strategy, and this strategy has applied in three-vector-based model predictive direct power control strategy for doubly fed induction generators, which can effectively reduce the switching losses of the inverter [14]. In [30], three additional auxiliary switches are adopted to reduce the switching losses of inverter; nevertheless, it not only increases the cost and complexity of the system, but also reduces the reliability of the system. A hybrid pulse-width-modulation technique is introduced in [31], which can effectively reduce current harmonic distortion and switching losses of the inverter. However, this offline optimization method is difficult to realize in real-time. In [32], the appropriate voltage vector sequence is selected online with the help of a predictive algorithm, and this selection is based on a cost function where users can define a tradeoff between the reduction of current distortion and switching losses. However, if the cost function contains both the current distortion and the switching losses, how to choose the weighting factor needs further research. In [33] and [34], the discontinuous pulse width modulation (DPWM) scheme is improved and optimized, which can effectively reduce the switching losses of the inverter, but it is more complicated to use in combination with FCS-MPC. In [35], a method called minimum-loss vector PWM (MLV-PWM) is proposed, the voltage vector sequence is selected in a way that the switching of a VSI leg does not happen during the phase-current maximum to reduce the switching losses.

In order to improve the steady-state performance and reduce the switching losses for a PMSM drive system, a modulated model-free predictive control with minimum switching losses (MSL-MMFPC) is proposed in this paper. Firstly, the predictive current vectors corresponding to the six active voltage vectors are calculated, and then two adjacent current vectors are selected based on the predefined first-level cost function. Then, by reasonably allocating the duty cycles of the two current vectors and the zero-current vector, the current vector at the next control period is equal to the reference current vector. Hence, the optimal voltage vector is obtained. Moreover, in order to keep optimal control performance also in over-modulation region, a new rotating coordinate frame is used to adjust the optimal voltage vector. Then, the second-level cost function is designed to select the optimal voltage vector sequence, so that the switching of a VSI leg does not happen during the phase-current maximum, which can reduce the switching losses of the inverter. Finally, the simulation and experimental results obtained from a SMPMSM drive system are presented to verify the effectiveness of the proposed control method.

II. THE ULTRA-LOCAL MODEL OF PMSM DRIVE SYSTEM

The ultra-local model [4] of a PMSM drive system in the synchronous rotating dq-axes is set up and given as

$$\begin{cases} \dfrac{di_d}{dt} = F_d + \alpha_d u_d \\ \dfrac{di_q}{dt} = F_q + \alpha_q u_q \end{cases} \tag{1}$$

where i_d and i_q are dq-axes stator currents. u_d and u_q represent dq-axes reference voltages. α_d and α_q represent the proportional coefficients of dq-axes reference voltages.

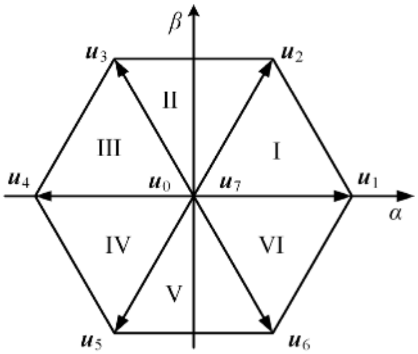

FIGURE 1. The distribution of space voltage vectors.

TABLE 1. Eight voltage vectors of the VSI.

Voltage vectors	State	S1	S3	S5
$\boldsymbol{u}_1$	1	1	0	0
$\boldsymbol{u}_2$	2	1	1	0
$\boldsymbol{u}_3$	3	0	1	0
$\boldsymbol{u}_4$	4	0	1	1
$\boldsymbol{u}_5$	5	0	0	1
$\boldsymbol{u}_6$	6	1	0	1
$\boldsymbol{u}_7$	7	1	1	1
$\boldsymbol{u}_0$	8	0	0	0

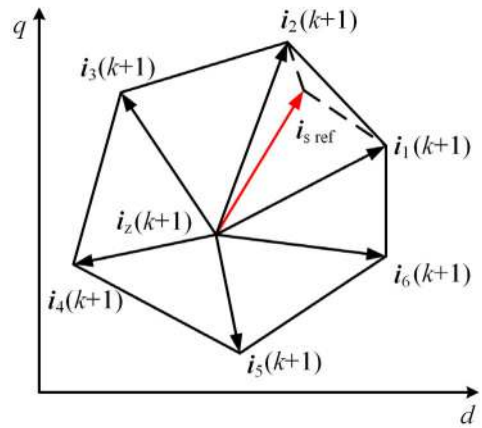

FIGURE 2. Predictive current vectors of eight basic voltage vectors and reference current vector in the *dq*-axes.

F_d and F_q contain the known and unknown parts of PMSM drive system.

The estimation of F_d and F_q can be obtained by the algebraic parameter identification techniques [5] and given as

$$\begin{cases} \hat{F}_d = -\dfrac{3!}{T_F^3}\int_0^{T_F}((T_F-2\delta)i_d(\delta) \\ \qquad +\alpha_d\delta(T_F-\delta)u_d(\delta))d\delta \\ \hat{F}_q = -\dfrac{3!}{T_F^3}\int_0^{T_F}((T_F-2\delta)i_q(\delta) \\ \qquad +\alpha_q\delta(T_F-\delta)u_q(\delta))d\delta \end{cases} \tag{2}$$

where $T_F = n_F T_s$ is the window sequence length. $\hat{F}_d$ and $\hat{F}_q$ are the estimation of F_d and F_q, which can be estimated by the data of $n_F + 1$ periods. T_s is the control period.

Based on the discretization of (1), the prediction of the *dq*-axes stator current of PMSM in the next control period can be expressed as

$$\begin{cases} i_d(k+1) = \left(\hat{F}_d(k) + \alpha_d u_d(k)\right)T_s + i_d(k) \\ i_q(k+1) = \left(\hat{F}_q(k) + \alpha_q u_q(k)\right)T_s + i_q(k) \end{cases} \tag{3}$$

where $i_d(k+1)$ and $i_q(k+1)$ represent the predictive values of the *dq*-axes stator current. (k) is the value in the (k)th control period.

III. THE PROPOSED MSL-MMFPC METHOD

A two-level VSI is used to control a PMSM, and it can generate eight basic voltage vectors as shown in Fig. 1. The switching states "1-6" represent six active voltage vectors and switching states "7" and "8" are zero voltage vectors. The distribution of space voltage vectors are shown as Fig. 1 and Table 1.

The conventional FCS-MPC predicts the future current values of the eight basic voltage vectors, and then the current tracking error is taken as the target to design the cost function, and the basic voltage vector that minimizes the current error is selected as the optimal voltage vector. In this paper, the *dq*-axes stator current tracking error is selected as the mian control target, and the first-level cost function is designed as

$$J_i^1 = (\boldsymbol{i}_{sref} - \boldsymbol{i}_i(k+1))^2 \tag{4}$$

where $i = 0, 1, 2, \ldots 7$ represent the eight basic voltage vectors. $\boldsymbol{i}_{sref}$ denote the *dq*-axes reference current, and $\boldsymbol{i}_{sref} = i_{dref} + ji_{qref}$, $\boldsymbol{i}_i(k+1) = i_{id}(k+1) + ji_{iq}(k+1)$.

The arrangement of the eight predictive current vectors corresponding to the eight voltage vectors in the *dq*-axes can be shown in Fig. 2, where the space predictive current vectors also form a hexagon. Since zero current vectors $\boldsymbol{i}_0(k+1)$, $\boldsymbol{i}_7(k+1)$ have the same effects on i_d and i_q, so the two zero current vectors are unified as $\boldsymbol{i}_z(k+1)$. The geometric meaning of the first-level cost function is the square of the distance from each predictive current vector to the reference value. As shown in Fig. 2, the square of distance between current vector $\boldsymbol{i}_2(k+1)$ and reference current vector $\boldsymbol{i}_{sref}$ is the smallest, so $\boldsymbol{u}_2$ is selected as the optimal voltage vector to be applied in the next control period in conventional FCS-MPC. However, the FCS-MPC cannot realize current no-error tracking, which will lead to high current ripple.

In order to realize current no-error tracking, three current vectors are used to synthesize the reference current vector. Firstly, the predictive current values of six active voltage vectors are calculated. Then, according to the estimated results of first-level cost function, two predictive current vectors with the smallest and second-smallest cost function can be determined and recorded as $\boldsymbol{i}_a(k+1)$ and $\boldsymbol{i}_b(k+1)$, respectively, moreover, $\boldsymbol{i}_a(k+1)$ and $\boldsymbol{i}_b(k+1)$ are adjacent. The voltage

TABLE 2. Six sectors determined by the boundaries vectors.

Sector	$\boldsymbol{u}_a$	$\boldsymbol{u}_b$
I	$\boldsymbol{u}_1$	$\boldsymbol{u}_2$
II	$\boldsymbol{u}_3$	$\boldsymbol{u}_2$
III	$\boldsymbol{u}_3$	$\boldsymbol{u}_4$
IV	$\boldsymbol{u}_5$	$\boldsymbol{u}_4$
V	$\boldsymbol{u}_5$	$\boldsymbol{u}_6$
VI	$\boldsymbol{u}_1$	$\boldsymbol{u}_6$

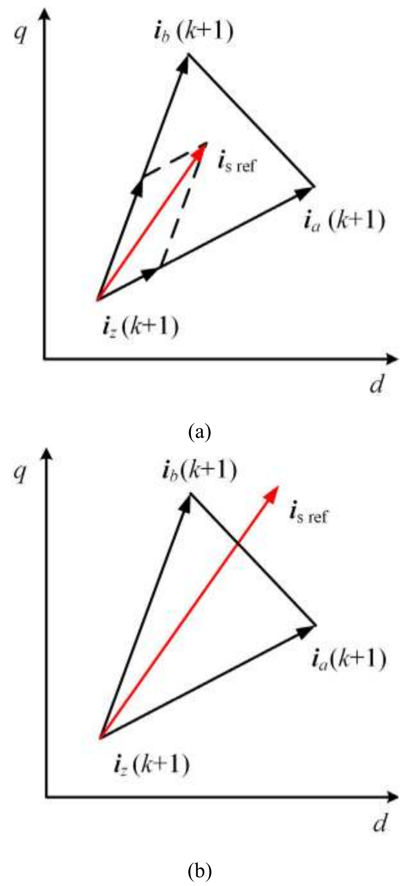

FIGURE 3. The two predictive current vectors in the *dq*-axes. (a) Linear modulation region. (b) Over-modulation region.

vectors corresponding to the selected predictive current vectors are $\boldsymbol{u}_a$ and $\boldsymbol{u}_b$ ($\boldsymbol{u}_a$ represents the active voltage vectors "$\boldsymbol{u}_1$", "$\boldsymbol{u}_3$" or "$\boldsymbol{u}_5$", $\boldsymbol{u}_b$ represents the active voltage vectors "$\boldsymbol{u}_2$", "$\boldsymbol{u}_4$" or "$\boldsymbol{u}_6$"), respectively. Taking $\boldsymbol{u}_a$ and $\boldsymbol{u}_b$ as the boundaries of sectors, the voltage vector space can be divided into six sectors, as shown in Table 2.

The arrangement of the selected two predictive current vectors in the dq-axes can be shown as in Fig. 3. In this plane, the two predictive current vectors and zero current vectors form a triangle. If the reference current vector $\boldsymbol{i}_{\text{sref}}$ is inside the triangle, the system operates in the linear modulation region, as is depicted in Fig. 3(a). In addition, if the reference current vector $\boldsymbol{i}_{\text{sref}}$ lies outside the triangle, as shown in Fig. 3(b), this corresponds to over-modulation operation. Both two cases are discussed in detail below.

A. DUTY CYCLES CALCULATION IN LINEAR MODULATION REGIOND

After determining the two current vectors, the duty cycle of each current vector can be calculated. The duty cycles of selected predictive current vectors $\boldsymbol{i}_a(k+1)$ and $\boldsymbol{i}_b(k+1)$ are denoted as d_a and d_b, respectively. The duty cycle of predictive zero current vector $\boldsymbol{i}_z(k+1)$ is denoted as d_z. The goal is to find a set of optimal solutions for duty cycle d_a, d_b and d_z of three predictive current vectors, so that the stator current can reach its reference value at the next control period.

Consequently, according to the geometric relationship as shown in Fig. 3(a), the duty cycles can be obtained by solving the following linear equations

$$d_a\left(\boldsymbol{i}_a(k+1)-\boldsymbol{i}_z(k+1)\right)+d_b\left(\boldsymbol{i}_b(k+1)-\boldsymbol{i}_z(k+1)\right) = \boldsymbol{i}_{\text{sref}}-\boldsymbol{i}_z(k+1) \tag{5}$$

And the duty cycles of three predictive current vectors are limited to

$$d_a+d_b+d_z=1 \tag{6}$$

According to (6), the components of predictive current vectors in (5) can be written on the dq-axes as

$$\begin{cases} i_{ad}(k+1)\cdot d_a+i_{bd}(k+1)\cdot d_b+i_{zd}(k+1)\cdot d_z=i_{d\text{ref}} \\ i_{aq}(k+1)\cdot d_a+i_{bq}(k+1)\cdot d_b+i_{zq}(k+1)\cdot d_z=i_{q\text{ref}} \\ d_a+d_b+d_z=1 \end{cases} \tag{7}$$

Solving the linear equations (7), the duty cycles of the three predictive current vectors d_a, d_b and d_z can be obtained. Therefore, by modulating the selected predictive current vector $\boldsymbol{i}_a(k+1)$, $\boldsymbol{i}_b(k+1)$ and predictive zero current vector $\boldsymbol{i}_z(k+1)$ properly, the current vector at the next control period is equal to the reference current vector. Consequently, the optimal voltage vector to be applied in the next control period is then given as

$$\boldsymbol{u}_{opt}=d_a\boldsymbol{u}_a+d_b\boldsymbol{u}_b \tag{8}$$

where $\boldsymbol{u}_a$ and $\boldsymbol{u}_b$ represent the active voltage vectors corresponding to the predictive current vectors $\boldsymbol{i}_a(k+1)$ and $\boldsymbol{i}_b(k+1)$.

B. DUTY CYCLES ADJUSTMENT IN OVER-MODULATION REGION

It must be noted that if $d_a+d_b>1$, it means the reference current vector is outside the triangle as shown in Fig. 3(b). This corresponds to over-modulation operation. In this case, the magnitude of the optimal voltage vector $\boldsymbol{u}_{opt}$ (red line) exceeds the voltage constraint in the $\alpha\beta$ stationary reference frame as shown in Fig. 4(a). Thus, the $\boldsymbol{u}_{opt}$ should be limited to the edge of the regular triangle formed by two adjacent active voltage vectors. In order to find the modified optimal

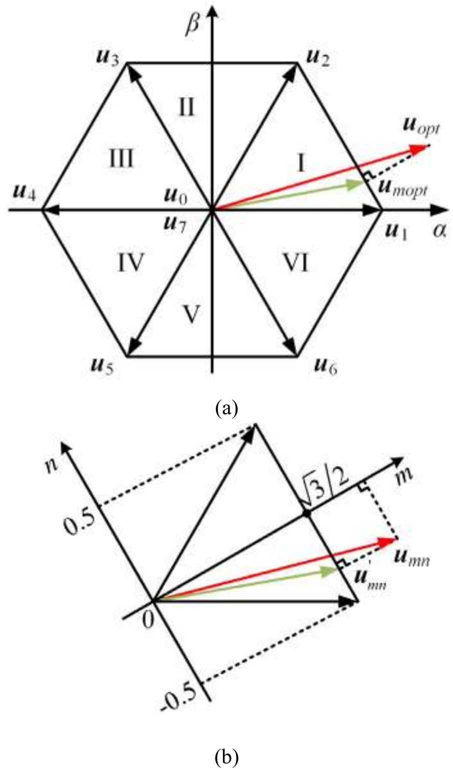

FIGURE 4. **Optimal voltage vector lies outside the triangle. (a) In the $\alpha\beta$-axes. (b) In the *mn*-axes.**

voltage vector, the best solution is to make the modified optimal voltage vector closest to the non-modified optimal voltage vector. As is illustrated in Fig. 4(a), when $\boldsymbol{u}_{opt}$ lies outside the triangle, it is projected perpendicularly to the edge of the triangle, resulting in $\boldsymbol{u}_{mopt}$(green line).

In order to obtain the projection more easily, a new *mn* rotating coordinate frame is set up, where the sector that $\boldsymbol{u}_{mn}$ located is centered at 0 degree in the *mn*-axes. As shown in Fig. 4(b), if $\boldsymbol{u}_{mn}$ is located in sector I, then rotate the *mn*-axes so that the *m*-axis is in the center of the sector I. The optimal voltage vector is modified in the *mn*-axes and then returned to $\alpha\beta$-axes. The manipulation is given as follows.

The $\boldsymbol{u}_{opt}$ in the $\alpha\beta$-axes is converted to the *mn*-axes and is given as

$$\boldsymbol{u}_{mn} = u_m + ju_n = \left(\frac{u_{opt}^{\alpha} + ju_{opt}^{\beta}}{2u_{dc}/3}\right) \cdot e^{j\theta} \tag{9}$$

where $\theta = (\pi\text{-}2\pi \cdot \text{Sector})/6$, u_{dc} is the DC-link voltage and $2u_{dc}/3$ is the amplitude of the active voltage vector.

Then, the u_m and u_n in the *mn*-axes are limited to

$$u'_m = \begin{cases} u_m, & u_m \leq \dfrac{\sqrt{3}}{2} \\ \dfrac{\sqrt{3}}{2}, & u_m > \dfrac{\sqrt{3}}{2} \end{cases} \tag{10}$$

$$u'_n = \begin{cases} u_n, & |u_n| \leq \dfrac{1}{2} \\ \dfrac{1}{2}\text{sign}(u_n), & |u_n| > \dfrac{1}{2} \end{cases} \tag{11}$$

TABLE 3. **The duty cycles in the over-modulation region.**

Sector	d_a	d_b
I	C_1-C_2	$2C_2$
II	-C_1+C_2	C_1+C_2
III	$2C_2$	-C_1-C_2
IV	-$2C_2$	-C_1+C_2
V	-C_1- C_2	C_1-C_2
VI	C_1+C_2	-$2C_2$

Finally, the modified voltage vector in the *mn*-axes is returned to $\alpha\beta$-axes.

$$\begin{aligned}\boldsymbol{u}_{mopt} &= \left(u_{mopt}^{\alpha} + ju_{mopt}^{\beta}\right) = \boldsymbol{u}'_{mn} \cdot \frac{2}{3}u_{dc} = \left(u'_m + ju'_n\right) \cdot \frac{2}{3}u_{dc} \\ &= \left(\frac{2u_{dc}(u'_m + ju'_n)}{3}\right) \cdot e^{-j\theta}\end{aligned} \tag{12}$$

When the optimal voltage vector is modified as $\boldsymbol{u}_{mopt}$ in the over-modulation region, the duty cycles of two active voltage vectors should be recalculate. For example, if the modified optimal voltage vector $\boldsymbol{u}_{mopt}$ lies inside the first sector, according to the principle of vector synthesis, $\boldsymbol{u}_{mopt}$ can be synthesized by two adjacent active voltage vectors $\boldsymbol{u}_1$ and $\boldsymbol{u}_2$.

$$\begin{cases} d_a\boldsymbol{u}_1^{\alpha} + d_b\boldsymbol{u}_2^{\alpha} = \boldsymbol{u}_{mopt}^{\alpha} \\ d_a\boldsymbol{u}_2^{\beta} + d_b\boldsymbol{u}_2^{\beta} = \boldsymbol{u}_{mopt}^{\beta} \end{cases} \tag{13}$$

where u_1^{α} and u_1^{β} are the values of the active voltage vector $\boldsymbol{u}_1$ in the $\alpha\beta$-axes; u_2^{α} and u_2^{β} are the values of the active voltage vector $\boldsymbol{u}_2$ in the $\alpha\beta$-axes;u_{mopt}^{α} and u_{mopt}^{β} are the values of the optimal voltage vector $\boldsymbol{u}_{mopt}$ in the $\alpha\beta$-axes.

Then, the duty cycles are calculated by

$$\begin{cases} d_a = \dfrac{3}{2U_{dc}}\left(u_{mopt}^{\alpha} - \dfrac{u_{mopt}^{\beta}}{\sqrt{3}}\right) \\ d_b = \dfrac{\sqrt{3}u_{mopt}^{\beta}}{U_{dc}} \end{cases} \tag{14}$$

Based on the above analysis, as shown in Table 3, the duty cycles of two adjacent active voltage vectors can be determined when $\boldsymbol{u}_{mopt}$ is in six sectors respectively.

where $C_1 = \frac{3u_{mopt}^{\alpha}}{2U_{dc}}$, $C_2 = \frac{\sqrt{3}\,u_{mopt}^{\beta}}{2U_{dc}}$, u_{mopt}^{α} and u_{mopt}^{β} are the values of the optimal voltage vector $\boldsymbol{u}_{mopt}$ in the $\alpha\beta$-axes.

C. VOLTAGE VECTOR SEQUENCE OPTIMIZATION BASED ON MINIMUM SWITCHING LOSSES

In seven-segment SVM strategy, the commutation of the voltage vector sequence is 6 times in one control period, and in five-segment SVM strategy, the voltage vector sequence reduces the commutation to 4 times. Thus, the five-segment SVM strategy (such as DPWMMIN) has the advantage of low switching frequency. Assuming that the optimal voltage

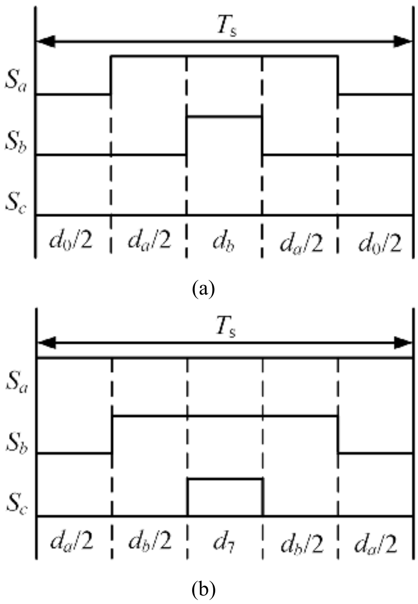

FIGURE 5. Switching sequences of the VSI. (a) u_0-u_a-u_b-u_a-u_0. (b) u_a-u_b-u_7-u_b-u_a.

vector is located in any sector, then the two adjacent active voltage vectors are selected as $\boldsymbol{u}_a$ and $\boldsymbol{u}_b$, and their duty cycles in one control period are d_a and d_b, respectively. The remaining time of the control period is filled with the zero voltage vector $\boldsymbol{u}_z$, and its duty cycle is d_z. The zero voltage vector can be selected from "000" or "111", and thus, the optimal voltage vector can be synthesized by the two clamping vector sequences $\{ab7ba\}$ and $\{0aba0\}$. Taking the first sector as an example, after determining the required active voltage vectors $\boldsymbol{u}_a$ and $\boldsymbol{u}_b$($\boldsymbol{u}_a$, $\boldsymbol{u}_b$ are $\boldsymbol{u}_1$, $\boldsymbol{u}_2$ respectively) and zero voltage vector $\boldsymbol{u}_z$, there are two candidate vector sequences as shown in Fig. 5. In the five-segment SVM strategy, only the vector sequence $\{0aba0\}$ is applied. In order to reduce the switching losses, the voltage vector sequence with minimum switching losses will be selected between two voltage vector sequences. The idea of MLV-PWM [35] is to select the appropriate zero voltage vector according to the sector where the optimal voltage vector is located. And in this way, the switching of a VSI leg does not happen during the phase-current maximum, and thus, leading to minimum switching losses.

The switching losses in the switching process during the control period T_s is the sum of the turn-on and turn-off switching losses E_{on} and E_{off} of each MOSFET and of the turn-off switching losses E_{offD} of each diode.

By assuming that E_{on}, E_{off}, and E_{offD} are proportional to the DC-link voltage U_{dc} and the phase current i, thus, their values are given as follows [36]

$$\begin{cases} E_{on} = \dfrac{1}{2}\dfrac{2E_{ontest}}{V_{test}I_{test}}iU_{dc} = \dfrac{t_{on}}{2}iU_{dc} \\ E_{off} = \dfrac{1}{2}\dfrac{2E_{offtest}}{V_{test}I_{test}}iU_{dc} = \dfrac{t_{off}}{2}iU_{dc} \\ E_{offD} = \dfrac{1}{2}\dfrac{2E_{offDtest}}{V_{test}I_{test}}iU_{dc} = \dfrac{t_{offD}}{2}iU_{dc} \end{cases} \tag{15}$$

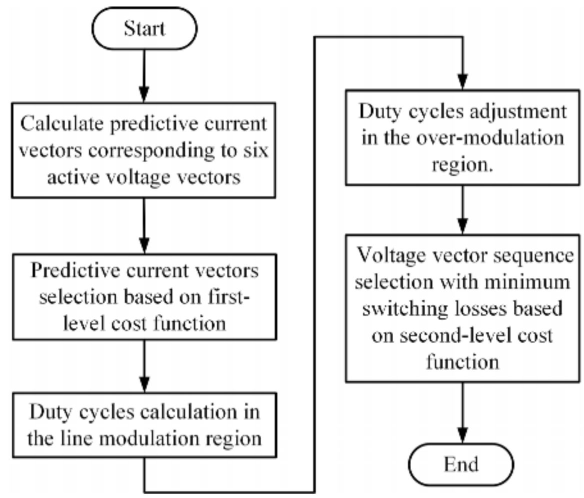

FIGURE 6. The flowchart of the proposed MSL-MMFPC method.

where E_{ontest}, $E_{offtest}$ and $E_{offDtest}$ are the switching losses in the test conditions; V_{test} and I_{test} are the voltage and current in the test conditions; t_{on} and t_{off} are the turn-on and turn-off times of the MOSFET, t_{offD} is the turn-off time of the diode. These values of t_{on}, t_{off} and t_{offD} are normally given in the datasheets.

To simplify the calculation process, the linear model between the switching losses and the phase current is used to estimate the turn-on and turn-off switching losses of the MOSFET. Therefore, according to (15) and the characteristics of the given voltage vector sequence, the average switching losses in a control period can be written as

$$P_{swj}(k+1) = \frac{1}{2T_s}\left(t_{on}+t_{off}+t_{offD}\right)U_{dc}\left(|i_{a1}(k)|+|i_{a2}(k)|\right) \tag{16}$$

where $j = 1, 2$ represent the two candidate clamping vector sequences $\{ab7ba\}$ and $\{0aba0\}$;$a1$, $a2$ denote the two non-clamped phase A, B or C on the control period.

Inspired by the thought of MLV-PWM, the appropriate zero voltage vector can be selected according to the switching losses of the inverter. Therefore, in order to select the optimal voltage vector sequence, the switching losses in the control period is taken as the target, and a second-level cost function is defined as

$$J_j^2 = P_{swj}(k+1) \quad j = 1, 2 \tag{17}$$

According to the evaluation result of the second-level cost function, the one which minimizes the switching losses is selected from the two candidate clamping vector sequences $\{ab7ba\}$ or $\{0aba0\}$.

IV. SYSTEM SIMULATION AND EXPERIMENTAL RESEARCH

A. SIMULATION RESEARCH

To validate effectiveness of the proposed MSL-MMFPC method, the PMSM drive system simulation model is established based on Matlab/Simulink. Fig. 6 shows the flowchart

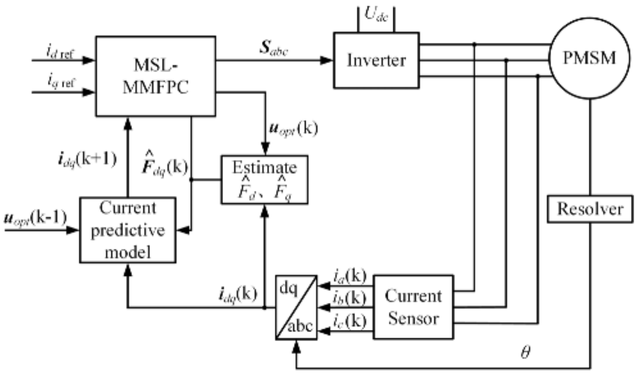

FIGURE 7. Control block diagram of the proposed MSL-MMFPC method.

TABLE 4. Parameters of tested SMPMSM.

Parameters	Value
Rated torque	13 N·m
Rated current (rms)	19 A
Rated speed	500 rpm
Stator resistance	0.0957 Ω
Stator inductance	1 mH
Magnet flux	0.027 Wb
Number of pole-pairs	12
Moment of inertia	0.01015 kg·m^2

of the proposed MSL-MMFPC method, and the control block diagram of the proposed MSL-MMFPC method is shown in Fig. 7. The conventional FCS-MPC method, MMFPC based on the five-segment SVM method (FS-MMFPC) and the proposed MSL-MMFPC method are compared. The sampling time of the conventional FCS-MPC method is set as $50\mu s$, and the other two methods are set as $100\mu s$. The inverter dead-time is set as $2\mu s$, and the DC-link voltage is 48V. The proportional coefficients of dq-axis reference voltages are chosen as $\alpha = \alpha_d = \alpha_q = 1/L_s = 1000$, and the window length n_F is set to 10. The nominal parameters of SMPMSM are given in Table 4.

To compare the dynamic and steady-state control performance, the step responses of q-axis stator current at 100rpm and 400rpm by three methods are shown in Fig. 8 and Fig. 9. The d-axis stator reference current $i_{d\text{ref}} = 0$A and q-axis stator reference current increases from 0A to 10A at $0.01s$. The drawings of partial enlargement in Fig. 8 and Fig. 9 show the dynamic performance of the system. All of three methods have the advantages of rapid dynamic performance and tracking their stator current reference value fastly. In addition, the FS-MMFPC method and the proposed MSL-MMFPC method have a small overshoot in the dynamic process because of the optimal voltage vector adjustment in the over-modulation region. Comparing the simulation results of steady-state control performance of three methods, the conventional FCS-MPC method presents large dq-axes stator current ripples, and the other two methods both have small dq-axes stator current ripples and excellent steady-state control performance.

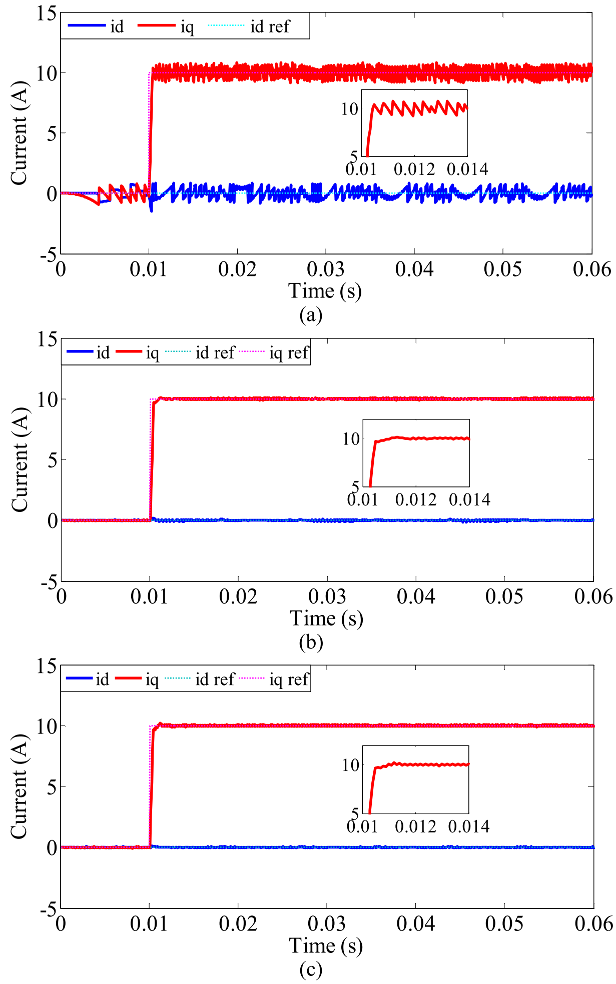

FIGURE 8. The dq-axes stator current response at 100rpm (simulation). (a) FCS-MPC. (b) FS-MMFPC. (c) MSL-MMFPC.

Fig. 10 and Fig. 11 show the simulation results of normalized A-phase current and duty cycle of A-phase at 100rpm and 300rpm of the two MMFPC methods, respectively. The duty cycles of A-phase equal to "0" or "1" means that the power device remains "ON" or "OFF" all the time, thus there are not switching actions. It is evident that the FS-MMFPC method does not have switching actions at the negative maximum value of A-phase current but still have switching actions at the positive maximum value. By contrast, the proposed MSL-MMFPC method has no switching actions either at the positive or the negative maximum value of A-phase current. Therefore, compared with the FS-MMFPC method, the proposed MSL-MMFPC method reduces the switching losses significantly.

B. EXPERIMENTAL RESEARCH

In order to verify the effectiveness of the proposed MSL-MMFPC method, an experimental prototype has been established as shown in Fig. 12, dSPACE/DS1007 is used

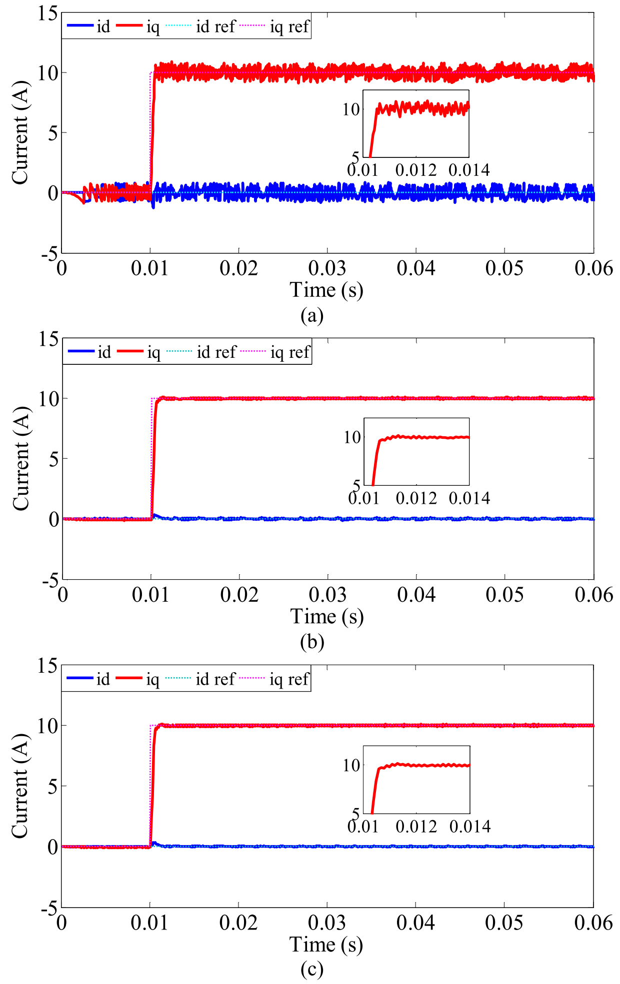

FIGURE 9. The *dq*-axes stator current response at 400rpm (simulation). (a) FCS-MPC. (b) FS-MMFPC. (c) MSL-MMFPC.

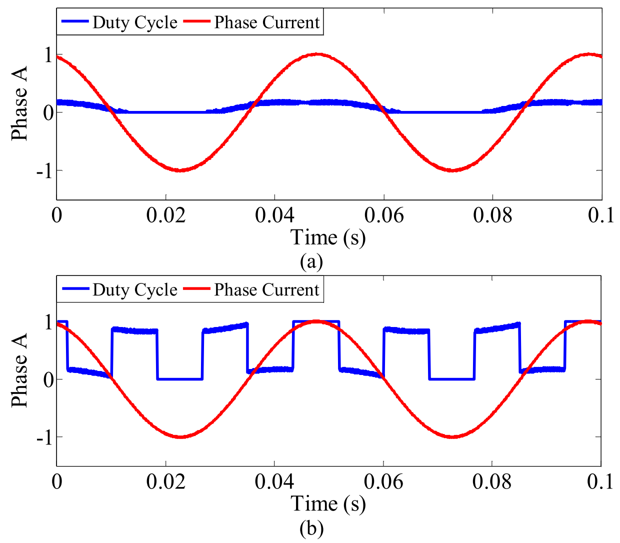

FIGURE 10. A-phase current and duty cycle of A-phase in steady-state operation at 100rpm (simulation). (a) FS-MMFPC. (b) MSL-MMFPC.

as the controller and generates the drive signal for the MOSFET-module inverter. The inverter dead-time is set as $2\mu s$. The resolver is used as the rotor position sensor,

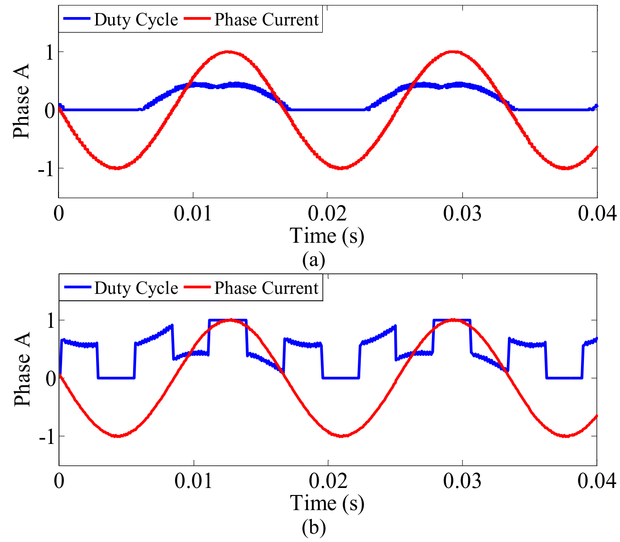

FIGURE 11. A-phase current and duty cycle of A-phase in steady-state operation at 300rpm (simulation). (a) FS-MMFPC. (b) MSL-MMFPC.

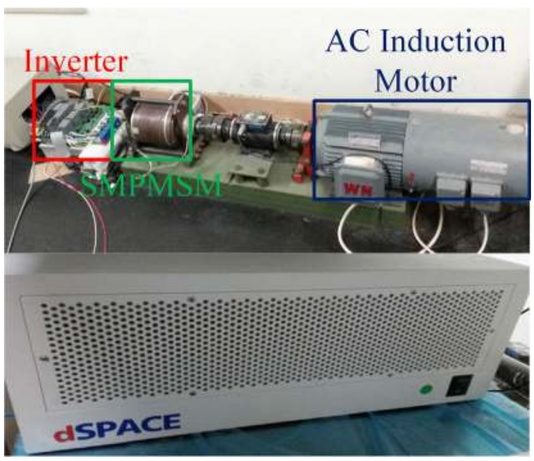

FIGURE 12. Experimental bench.

and the stator current is detected by a Hall-effect current sensor. The dynamometer is a 2.2kW AC induction-motor that operates in speed control mode. The sampling time of the conventional FCS-MPC method is set as $50\mu s$, and the other two methods are $100\mu s$. The nominal parameters of SMPMSM and the control parameters are the same as simulation.

In the experiment, the q-axis stator current step responses of the proposed MSL-MMFPC method are implemented at 100rpm and 400rpm, as shown in Fig. 13 and Fig. 14. The d-axis current $i_{dref} = 0$A and the q-axis current i_{qref} changes from 0A to 10A at $0.1s$. From the enlarged drawings of Fig. 13 and Fig. 14, three methods can obtain extremely quick dynamic response and the difference among them is not significant. Moreover, the FS-MMFPC method and the proposed MSL-MMFPC method achieve accurate current tracking performance with small overshoot. This is because those two MMFPC methods are based on predictive control and adjust the optimal voltage vector in the over-modulation region.

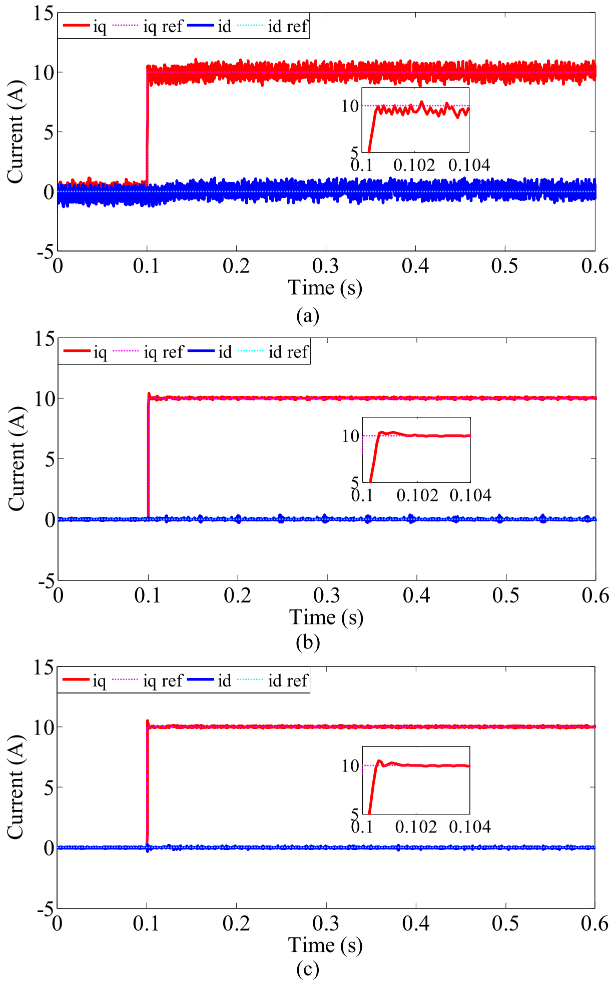

FIGURE 13. The *dq*-axes stator current response at 100rpm (experiment). (a) FCS-MPC. (b) FS-MMFPC. (c) MSL-MMFPC.

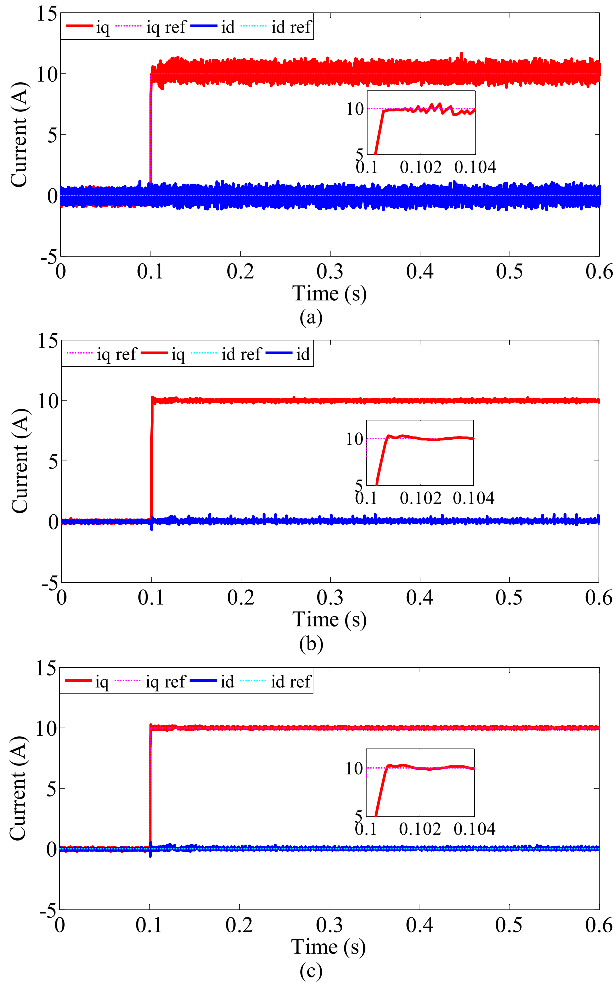

FIGURE 14. The *dq*-axes stator current response at 400rpm (experiment). (a) FCS-MPC. (b) FS-MMFPC. (c) MSL-MMFPC.

It can be seen from Fig. 13 and Fig. 14, the FS-MMFPC method and the proposed MSL-MMFPC method have similar steady-state control performance, and the *dq*-axes current ripples of both two methods are much lower than the conventional FCS-MPC method. The results are consistent with the simulation and this illustrates that both two MMFPC methods can obtain the optimal voltage vector, moreover, it can effectively improve the current steady-state response. Furthermore, the selection of different voltage vector sequence has little effect on the steady-state performance of the system.

Fig. 15 and Fig. 16 show the experimental results of normalized A-phase current and duty cycle of A- phase at100rpm and 300rpm of the two MMFPC methods, respectively. It can be seen from Fig. 15(a) and Fig. 16(a), there are still switching actions at the positive maximum value of A-phase current in the FS-MMFPC method. By comparison, one can see there are not switching actions at the positive or negative maximum value of A-phase current in the proposed MSL-MMFPC method. And hence, the switching losses will be greatly reduced. Furthermore, as we can see from Fig. 15 and Fig. 16, the peak value of A-phase current will shift to the right slightly with the increase of motor speed, but this has a limited effect on switching losses reduction.

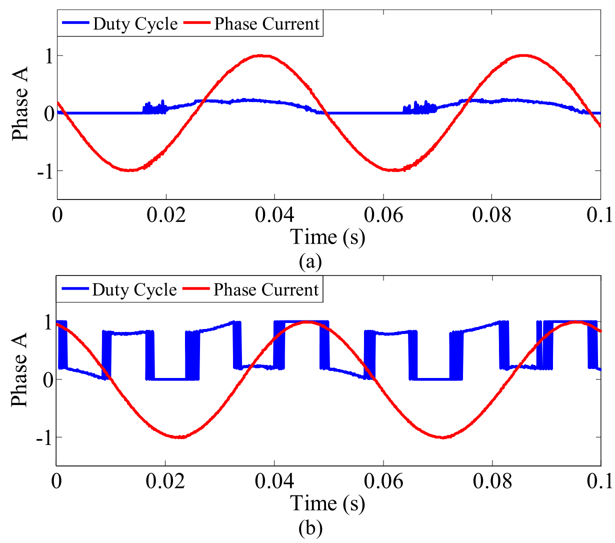

FIGURE 15. A-phase current and duty cycle of A-phase in steady-state operation at 100rpm (experiment). (a) FS-MMFPC. (b) MSL-MMFPC.

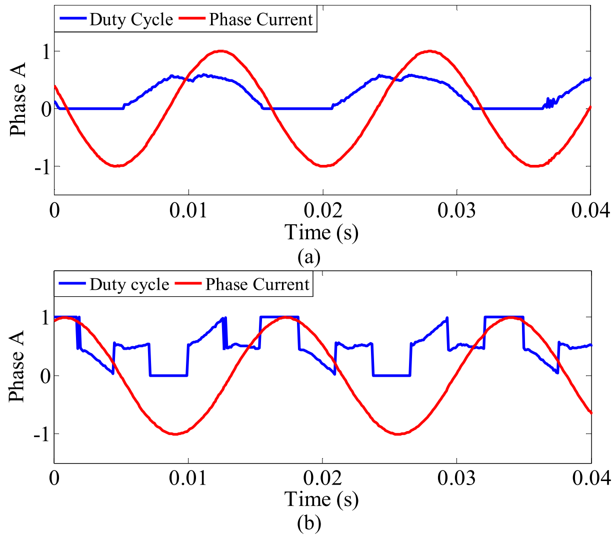

FIGURE 16. A-phase current and duty cycle of A-phase in steady-state operation at 300rpm (experiment). (a) FS-MMFPC. (b) MSL-MMFPC.

To further explore the steady-state performance and switching losses of the FS-MMFPC method and the proposed MSL-MMFPC method, a comparison of the A-phase current THD and switching losses of the inverter at different rotating speeds are implemented. In the experiments, the dq-axes reference currents are $i_{d\text{ref}} = 0$A and $i_{q\text{ref}} = 10$A.

The switching losses of the FS-MMFPC method and the proposed MSL-MMFPC method are compared by defining a switching loss function (SLF) as follows

$$SLF = \frac{P_{MSL-MMFPC}}{P_{FS-MMFPC}} \tag{18}$$

where $P_{FS-MMFPC}$ and $P_{MSL-MMFPC}$ are the switching losses of the FS-MMFPC method and the proposed MSL-MMFPC method, respectively.

The $P_{FS-MMFPC}$ and $P_{MSL-MMFPC}$ can be calculated as

$$\begin{cases} P_{FS-MMFPC} = \dfrac{1}{M}\sum\limits_{m=1}^{M} P_{sw\_FS-MMFPC}(m) \\ P_{MSL-MMFPC} = \dfrac{1}{M}\sum\limits_{m=1}^{M} P_{sw\_MSL-MMFPC}(m) \end{cases} \tag{19}$$

where $P_{FS-MMFPC}(m)$ and $P_{MSL-MMFPC}$ (m) are the switching losses of the FS-MMFPC method and the proposed MSL-MMFPC method in each control period, respectively. The value of M is 100,000.

Experimental results are shown in Table 5. Obviously, although the THD of the proposed MSL-MMFPC method is slightly higher than that of the FS-MMFPC method at different rotating speeds, the switching losses of the proposed MSL-MMFPC method is significantly reduced. The proposed MSL-MMFPC method can effectively reduce the switching losses of the inverter without sacrificing the steady-state control performance of the system.

The experimental results confirm again that the proposed MSL-MMFPC method can obtain the optimal voltage vector, so it can effectively improve the performance of the current steady-state and dynamic response. Moreover, compared with the FS-MMFPC method, it reduces the switching losses of the inverter effectively.

TABLE 5. Comparison of the A-phase current THD and the switching losses.

Speed (rpm)	THD (%) (FS-MMFPC)	THD (%) (MSL-MMFPC)	*SLF*
100	2.66	2.80	0.7501
200	2.10	2.52	0.7514
300	2.27	2.52	0.7575
400	2.68	2.74	0.7713
500	2.15	2.18	0.7727

V. CONCLUSION

This paper proposes a modulated model-free predictive control with minimum switching losses for PMSM drive systems. The six active current vectors are calculated based on the ultra-local model of PMSM drive system, and then two adjacent current vectors are selected based on the predefined first-level cost function. The optimal voltage vector is obtained by allocating the duty cycles of the selected two current vectors and zero current vectors reasonably. Compared with three-vector control, it is not necessary to calculate the duty cycles of voltage vector in all six sectors. Moreover, a new rotating coordinate frame is used to adjust the optimal voltage vector to improve the dynamic performance when VSI operates in the over-modulation region. Then, the second-level cost function is designed to select the optimal voltage vector sequence, in this way, the switching of a VSI leg does not happen during the phase-current maximum. Compared with the conventional FCS-MPC method, the dq-axes stator current ripples can be significantly reduced. Furthermore, compared with the FS-MMFPC method, the proposed MSL-MMFPC method reduces the switching losses effectively without affecting the steady-state control performance.

REFERENCES

[1] Y. Zhang, D. Xu, J. Liu, S. Gao, and W. Xu, "Performance improvement of model predictive current control of permanent magnet synchronous motor drives," *IEEE Trans. Ind. Electron.*, vol. 53, no. 4, pp. 3683–3695, Jul./Aug. 2017.

[2] S. Vazquez, R. P. Aguilera, P. Acuna, J. Pou, J. I. Leon, L. G. Franquelo, and V. G. Agelidis, "Model predictive control for single-phase NPC converters based on optimal switching sequences," *IEEE Trans. Ind. Electron.*, vol. 63, no. 12, pp. 7533–7541, Dec. 2016.

[3] N. Panten, N. Hoffmann, and F. W. Fuchs, "Finite control set model predictive current control for grid-connected voltage-source converters with LCL filters: A study based on different state feedbacks," *IEEE Trans. Power Electron.*, vol. 31, no. 7, pp. 5189–5200, Jul. 2016.

[4] M. Fliess and C. Join, "Model-free control," *Int. J. Control*, vol. 86, no. 12, pp. 2228–2252, Jul. 2013.

[5] Y. Zhou, H. Li, and H. Zhang, "Model-free deadbeat predictive current control of a surface-mounted permanent magnet synchronous motor drive system," *J. Power Electron.*, vol. 18, no. 1, pp. 103–115, Jan. 2018.

[6] Y. Zhang, Y. Peng, and H. Yang, "Performance improvement of two-vectors-based model predictive control of PWM rectifier," *IEEE Trans. Power Electron.*, vol. 31, no. 8, pp. 6016–6030, Aug. 2016.
[7] Y. Zhang, Y. Bai, and H. Yang, "A universal multiple-vector-based model predictive control of induction motor drives," *IEEE Trans. Power Electron.*, vol. 33, no. 8, pp. 6957–6969, Aug. 2018.
[8] S. Vazquez, J. Rodriguez, M. Rivera, L. G. Franquelo, and M. Norambuena, "Model predictive control for power converters and drives: Advances and trends," *IEEE Trans. Ind. Electron.*, vol. 64, no. 2, pp. 935–947, Feb. 2017.
[9] S. Vazquez, C. Montero, C. Bordons, and L. G. Franquelo, "Model predictive control of a VSI with long prediction horizon," in *Proc. IEEE Int. Symp. Ind. Electron.*, Jun. 2011, pp. 1805–1810.
[10] P. Karamanakos, T. Geyer, and R. P. Aguilera, "Long-horizon direct model predictive control: Modified sphere decoding for transient operation," *IEEE Trans. Ind. Appl.*, vol. 54, no. 6, pp. 6060–6070, Nov. 2018.
[11] Y. Zhang and H. Yang, "Model predictive torque control of induction motor drives with optimal duty cycle control," *IEEE Trans. Power Electron.*, vol. 29, no. 12, pp. 6593–6603, Dec. 2014.
[12] W. Chen, S. Zeng, G. Zhang, T. Shi, and C. Xia, "A modified double vectors model predictive torque control of permanent magnet synchronous motor," *IEEE Trans. Power Electron.*, vol. 34, no. 11, pp. 11419–11428, Nov. 2019.
[13] S. Vazquez, A. Marquez, R. Aguilera, D. Quevedo, J. I. Leon, and L. G. Franquelo, "Predictive optimal switching sequence direct power control for grid-connected power converters," *IEEE Trans. Ind. Electron.*, vol. 62, no. 4, pp. 2010–2020, Apr. 2015.
[14] X. Wang and D. Sun, "Three-vector-based low-complexity model predictive direct power control strategy for doubly fed induction generators," *IEEE Trans. Power Electron.*, vol. 32, no. 1, pp. 773–782, Jan. 2017.
[15] Q. Liu and K. Hameyer, "Torque ripple minimization for direct torque control of PMSM with modified FCSMPC," *IEEE Trans. Ind. Appl.*, vol. 52, no. 6, pp. 4855–4864, Nov. 2016.
[16] H. Li, M. Lin, M. Yin, J. Ai, and W. Le, "Three-vector-based low-complexity model predictive direct power control strategy for PWM rectifier without voltage sensors," *IEEE J. Emerg. Sel. Topics Power Electron.*, vol. 7, no. 1, pp. 240–251, Mar. 2019.
[17] X. Zhang, B. Hou, and Y. Mei, "Deadbeat predictive current control of permanent-magnet synchronous motors with stator current and disturbance observer," *IEEE Trans. Power Electron.*, vol. 32, no. 5, pp. 3818–3834, May 2017.
[18] L. Tarisciotti, P. Zanchetta, A. Watson, P. Wheeler, J. C. Clare, and S. Bifaretti, "Multi-objective modulated model predictive control for a multilevel solid state transformer," *IEEE Trans. Ind. Appl.*, vol. 51, no. 5, pp. 4051–4060, Sep./Oct. 2015.
[19] M. Rivera, F. Morales, C. Baier, J. Munoz, L. Tarisciotti, P. Zanchetta, and P. Wheeler, "A modulated model predictive control scheme for a two-level voltage source inverter," in *Proc. IEEE Int. Conf. Ind. Technol. (ICIT)*, Mar. 2015, pp. 2224–2229.
[20] A. Olloqui, J. L. Elizondo, M. Rivera, M. E. Macias, O. M. Micheloud, R. Pena, and P. Wheeler, "Modulated model predictive rotor current control (M2PC) of a DFIG driven by an indirect matrix converter with fixed switching frequency," in *Proc. IEEE 2nd Annu. Southern Power Electron. Conf. (SPEC)*, Dec. 2016, pp. 1–6.
[21] L. Tarisciotti, A. Formentini, A. Gaeta, M. Degano, P. Zanchetta, R. Rabbeni, and M. Pucci, "Model predictive control for shunt active filters with fixed switching frequency," *IEEE Trans. Ind. Appl.*, vol. 53, no. 1, pp. 296–304, Jan. 2017.
[22] M. Vijayagopal, P. Zanchetta, L. Empringham, L. De Lillo, L. Tarisciotti, and P. Wheeler, "Control of a direct matrix converter with modulated model-predictive control," *IEEE Trans. Ind. Appl.*, vol. 53, no. 3, pp. 2342–2349, May 2017.
[23] L. Tarisciotti, J. Lei, A. Formentini, A. Trentin, P. Zanchetta, P. Wheeler, and M. Rivera, "Modulated predictive control for indirect matrix converter," *IEEE Trans. Ind. Appl.*, vol. 53, no. 5, pp. 4644–4654, Sep. 2017.
[24] F. Zhang, T. Peng, H. Dan, J. Lin, and M. Su, "Modulated model predictive control of permanent magnet synchronous motor," in *Proc. IEEE Int. Conf. Ind. Electron. Sustain. Energy Syst. (IESES)*, Jan. 2018, pp. 130–133.
[25] X. Li, T. Peng, H. Dan, G. Zhang, W. Tang, W. Jin, P. Wheeler, and M. Rivera, "A modulated model predictive control scheme for the brushless doubly-fed induction machine," *IEEE Trans. Emerg. Sel. Topics Power Electron.*, vol. 6, no. 4, pp. 1681–1691, Dec. 2018.
[26] Y. Yang, H. Wen, and D. Li, "A fast and fixed switching frequency model predictive control with delay compensation for three-phase inverters," *IEEE Access*, vol. 5, pp. 17904–17913, 2017.
[27] L. Tarisciotti, P. Zanchetta, A. Watson, J. C. Clare, M. Degano, and S. Bifaretti, "Modulated model predictive control for a three-phase active rectifier," *IEEE Trans. Ind. Appl.*, vol. 51, no. 2, pp. 1610–1620, Mar. 2015.
[28] S. S. Yeoh, T. Yang, L. Tarisciotti, C. I. Hill, S. Bozhko, and P. Zanchetta, "Permanent-magnet machine-based starter–generator system with modulated model predictive control," *IEEE Trans. Transport. Electrific.*, vol. 3, no. 4, pp. 878–890, Dec. 2017.
[29] E. Fuentes, C. A. Silva, and R. M. Kennel, "MPC implementation of a quasi-time-optimal speed control for a PMSM drive, with inner modulated-FS-MPC torque control," *IEEE Trans. Ind. Electron.*, vol. 63, no. 6, pp. 3897–3905, Jun. 2016.
[30] Y. Li, F. Lee, and D. Boroyevich, "A simplified three-phase zero-current-transition inverter with three auxiliary switches," *IEEE Trans. Power Electron.*, vol. 18, no. 3, pp. 802–813, May 2003.
[31] D. Zhao, V. S. S. P. K. Hari, G. Narayanan, and R. Ayyanar, "Space-vector-based hybrid pulsewidth modulation techniques for reduced harmonic distortion and switching loss," *IEEE Trans. Power Electron.*, vol. 25, no. 3, pp. 760–774, Mar. 2010.
[32] M. Gendrin, J.-Y. Gauthier, and X. Lin-Shi, "A predictive hybrid pulse-width-modulation technique for active-front-end rectifiers," *IEEE Trans. Power Electron.*, vol. 32, no. 7, pp. 5487–5496, Jul. 2017.
[33] N.-V. Nguyen, B.-X. Nguyen, and H.-H. Lee, "An optimized discontinuous PWM method to minimize switching loss for multilevel inverters," *IEEE Trans. Ind. Electron.*, vol. 58, no. 9, pp. 3958–3966, Sep. 2011.
[34] S. Mukherjee, S. K. Giri, S. Kundu, and S. Banerjee, "A generalized discontinuous PWM scheme for three-level NPC traction inverter with minimum switching loss for electric vehicles," *IEEE Trans. Ind. Appl.*, vol. 55, no. 1, pp. 516–528, Jan. 2019.
[35] A. M. Trzynadlowski and S. Legowski, "Minimum-loss vector strategy for three phase inverters," *IEEE Trans. Power Electron.*, vol. 9, no. 1, pp. 26–34, Jan. 1994.
[36] S. C. Das, G. Narayanan, and A. Tiwari, "Variation of IGBT switching energy loss with device current: An experimental investigation," in *Proc. IEEE 6th India Int. Conf. Power Electron. (IICPE)*, Dec. 2014, pp. 1–5.

YUCHEN WANG was born in Anhui, China, in 1994. He received the B.S. degree in electrical engineering and automation from Tongling University, in 2017. He is currently pursuing the M.S. degree with the Department of Electrical Engineering and Automation, Hefei University of Technology, Hefei, China. His current research interest includes power electronics and predictive control of electrical motor drives.

HONGMEI LI was born in Anhui, China, in 1969. She received the B.S. and M.S. degrees in electrical engineering from the Hefei University of Technology, Hefei, China, in 1991 and 1996, respectively, and the Ph.D. degree in electrical engineering from the Shenyang University of Technology, Shenyang, China, in 2003. She has been working as a Professor at the Department of Electrical Engineering, Hefei University of Technology, since 2006. Her current research interests include power electronics and motor control, predictive control, and the fault-tolerant control of electrical machine systems.

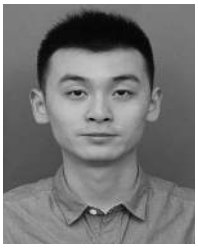

RUNDONG LIU was born in Anhui, China, in 1989. He received the B.S. degree in automation from Anhui Polytechnic University, Wuhu, China, in 2011, and the M.S. degree in electrical engineering from the Hefei University of Technology, Hefei, China, in 2018, where he is currently pursuing the Ph.D. degree with the Department of Electrical Engineering and Automation. His research interest includes predictive control and model-free control of electrical motor drives.

LIGUO YANG was born in Shanxi, China, in 1996. He received the B.S. degree from the Shenyang University of Technology, Shenyang, China, in 2018. He is currently pursuing the master's degree with the Department of Electrical Engineering and Automation, Hefei University of Technology. His research interest includes predictive control for electrical drives.

XIANLING WANG was born in Anhui, China, in 1995. She received the B.S. degree in electrical engineering and automation from the Wuhan University of Technology, in 2017. She is currently pursuing the M.S. degree with the Department of Electrical Engineering and Automation, Hefei University of Technology. Her current research interest includes power electronics and predictive control of electrical motor drives.